ELSEVIER

Earth and Planetary Science Letters 199 (2002) 359–372

EPSL

www.elsevier.com/locate/epsl

A multibeam-sonar, magnetic and geochemical flowline survey at 14°14′S on the southern East Pacific Rise: insights into the fourth dimension of ridge crest segmentation

Ingo Grevemeyer [a,*], Burkhard Schramm [a], Colin W. Devey [a], Douglas S. Wilson [b], Birgit Jochum [c], Jan Hauschild [a], Kay Aric [c], Heinrich W. Villinger [a], Wilfried Weigel [d]

[a] *Department of Earth Sciences, University of Bremen, Klagenfurter Straße, 28359 Bremen, Germany*
[b] *Department of Geological Sciences and Marine Institute, University of California, Santa Barbara, CA 93106, USA*
[c] *Institute of Meteorology and Geophysics, University of Vienna, Althanstraße, 1000 Vienna, Austria*
[d] *Institute of Geophysics, University of Hamburg, Bundesstraße 55, 20146 Hamburg, Germany*

Received 4 February 2002; received in revised form 6 March 2002; accepted 11 March 2002

Abstract

A detailed bathymetric and magnetic survey of the eastern flank of the East Pacific Rise at 14°14′S covering seafloor ages of 0–10 Ma has been carried out and used, along with a flowline profile on the conjugate western ridge flank, to reveal the spreading history and the temporal ridge crest segmentation. Additional information from basaltic lavas is included to study the relationship between physical and magmatic segment boundaries. The sequence of magnetic reversals indicates a total spreading rate of 150 mm/yr since 10 Ma. Symmetric spreading, however, occurred only since 2.8 Ma. Between 7 and 2.8 Ma spreading was asymmetric, with a higher spreading rate toward the east. Migration events of at least five overlapping spreading centres (OSC) left discordant zones on the Nazca plate consisting of hummocky basins and motley texture of curved lineations striking a few degrees oblique to the strike of the ridge crest. Four of the OSCs were right-stepping and migrated northward and one was left-stepping and migrated southward. By transferring Pacific lithosphere to the Nazca plate, these migration events may account for most of the asymmetric accretion observed. The basaltic samples from the eastern flank have been analysed and back tracked to the position of eruption on the ridge crest. In terms of their geochemical signature (Mg# 0.41–0.68) the samples reveal that the magmatic segment boundary between the Garrett transform and 14°30′S has remained stationary over the last 10 Myr and therefore provide no evidence for a link between magmatic and physical segmentation. We therefore propose that migrating non-transform ridge axis discontinuities are governed by propagating giant cracks; as a crack front advances a melt reservoir is tapped and magma rises passively into the crack and erupts subsequently on the seafloor. Some of the OSCs seem to have originated close to transform faults and therefore argue that far-field stresses, perhaps caused by the evolution of the Bauer microplate, rather than mantle upwelling create non-transform ridge axis discontinuities.

* Corresponding author. Tel.: +49-421-218-4511; Fax: +49-421-218-7163.
E-mail address: ingo@geophys2.uni-bremen.de (I. Grevemeyer).

0012-821X/02/$ – see front matter
PII: S0012-821X(02)00595-2

Keywords: East Pacific Rise; mid-ocean ridges segmentation; bathymetry; reversals; major elements

1. Introduction

Observations along the approximately 70 000 km long mid-ocean ridge system support the concept of a hierarchy in the segmentation of spreading ridges [1–3]. Discontinuities that define first-order segments are rigid and long-lived transform faults, whereas finer scales of segmentation occur between transform faults. At fast spreading ridges, lateral offsets of 1–30 km occur at second- and third-order discontinuities and are accommodated by overlapping spreading centres (OSC). Fourth-order discontinuities are minor deviations in axial linearity (DEVAL) with offsets of less than 1 km. At higher orders, segments are shorter, more short-lived, and unstable [4].

Off-axis traces of ridge axis discontinuities are created at first- and second-order segment boundaries. Transverse ridges and fracture zone valleys of transform fault boundaries have even been imaged by satellite-borne altimeters [5]. Recent multibeam-sonar surveys of mid-ocean ridges reveal off-axis discordant zones related to non-transform ridge axis discontinuities at both slow and fast spreading ridges [4,6,7]. The off-axis discordant zones of second-order discontinuities reveal the history of segment evolution and magmatic activity. At fast spreading ridges many show a pattern of abandoned ridge tips and fossil overlap basins caused by repeated decapitation of ridge tips. Such propagation and decapitation events have a recurrence interval of 2×10^4–2×10^5 yr with an average interval of $\sim5\times10^4$ yr [4,8]. The lack of any off-axis discordant zone documents the short-lived nature of third- and fourth-order segments relative to the larger, longer-lived discontinuities.

Seismic measurements along the axis of the East Pacific Rise (EPR) reveal an axial magma chamber (AMC) whose shape and position correlate with the shape of the rise [8]. The AMC disappears near transform faults, is deeper and commonly discontinuous near second-order discontinuities, and it shows only small variations at third- and some fourth-order discontinuities [9]. These observations suggest a linkage between tectonic segmentation and the axial melt reservoir. Langmuir et al. [1] show that volcanic rocks at broader and hence magmatically robust segments [8] have higher MgO content than those from the narrower parts of segments, generally near discontinuities. The data are, however, sparse and noisy. Nevertheless, they suggest a tendency for hotter magmas to erupt near the middle of segments and cooler magmas to erupt near segment ends. Within the resolution of sampling, virtually all segments of order 1–3 have distinct geochemical signatures, as do at least 30% of the fourth-order segments [1,10]. Some authors argue that spreading segments behave like giant cracks in the plate [4,11], however. In this case tectonic segment boundaries are not necessarily prone to coincide with magmatic segment boundaries which may explain why the correspondence between geochemical and geophysical segmentation is imperfect.

Flowline studies crossing abandoned ridge tips have the potential to be able to tell us more about the linkage between physical and magmatic segmentation of ridge crests. During the EXCO surveys in 1995 and 2000 [12–15] the German research vessel *Sonne* investigated a flowline corridor centred at 14°14′S on the southern East Pacific Rise (SEPR) (Fig. 1). This portion of the SEPR is known to be among the most robust and magmatically active portions of the world's mid-ocean ridge system [8,16,17]. Here we use HYDROSWEEP multibeam bathymetry and magnetic coverage of a 40–80 km wide and 720 km long tectonic corridor on the eastern ridge flank along with a conjugate flowline profile on the western flank and geochemical information on basaltic lavas from the eastern flank to reveal the tectonic and magmatic evolution of the SEPR at 14°14′S since 10 Ma.

2. Geological background

The Southern East Pacific Rise between the

Fig. 1. Location map showing the survey area of research vessel *Sonne* in 1995 and 2000 in the south-east Pacific ocean on the East Pacific Rise.

Easter Microplate near 23°S and the Garrett transform fault boundary near 13°30′S is spreading at ultrafast rates, ranging from 143 mm/yr to 150 mm/yr [18,19]. Between the Garrett fracture zone and a large duelling OSC at 20°40′S the SEPR is remarkably linear and devoid of any transform fault boundaries [20]. On a finer scale, however, the ridge crest is offset en echelon by a series of small, left stepping discontinuities [7,20]. These discontinuities range in offset from 1 to 7 km, and the intervening ridge segments consistently strike within a few degrees of 013°, normal to the spreading direction predicted by the NUVEL-1A model of current plate motions [18,19]. In addition, all second-order physical ridge offsets seem to correspond to magmatic segment boundaries defined by the ratio of K/P and K/Ti of glass [10]. Along this portion of the ridge crest five regions with relatively smooth variation in MgO contents are apparent [10]. Most of the boundaries of these regions correspond to major physical or secondary magmatic boundaries. Nevertheless, two occur within secondary magmatic segments near small offset non-transform ridge axis discontinuities.

Between 16°S and 21°S the SEPR has been intensively studied by combined multibeam, side scan and magnetic surveys. Off-axis discordant zones reveal that between 1 and 5 Ma several left-stepping OSCs offset the ridge axis between 16°S and 19°S. Since 1 Ma these OSCs were bisected into smaller OSCs by new spreading segments forming within their overlap basins [19,21]. The smaller OSCs migrated rapidly southward and were further bisected until the present segmentation was achieved. By transferring lithosphere from one plate to the other, these migration and reorientation events account remarkably well for the spreading asymmetry along the SEPR. The large OSC at 20°40′S has remained stationary since 1 Ma, but its history involves duelling propagation with a great deal of variation in the amount of overlap of the two ridges as well as inward and outward cutting and abandonment of tips of both ridges [22,23].

In general, along axis variations of several physical and chemical parameters in this area suggest that the melt supply to the ridge is robust between the Garrett transform fault and the duelling OSC at 20°40′S. At 14°14′S the ridge crest is characterized by a prominent bathymetric high with smooth flanks and a relatively flat summit [8,20]. Seismic reflection imaging provides evidence for an axial magma chamber reflector [16,17]. Both the blocky crestal ridge and the prominent AMC reflector are consistent with a magmatically active ridge segment [8,16]. Moreover, the seismic data indicate a very uniform process of crustal accretion along axis [16,17]. Off-axis, Grevemeyer et al. [13] investigated the seafloor morphology and found that changes in seafloor roughness and abundance and height of seamounts correlate with temporal changes in spreading rate. Over the last 10 Myr, however, crustal accretion has produced a quite uniform crustal thickness [24] which argues for only minor changes in melt supply.

3. Data collection and processing

Most of the bathymetric and magnetic data have been acquired during leg 105 of the *Sonne* in 1995. Data covering a 20–45 km wide and 720 km long corridor on the eastern flank were ini-

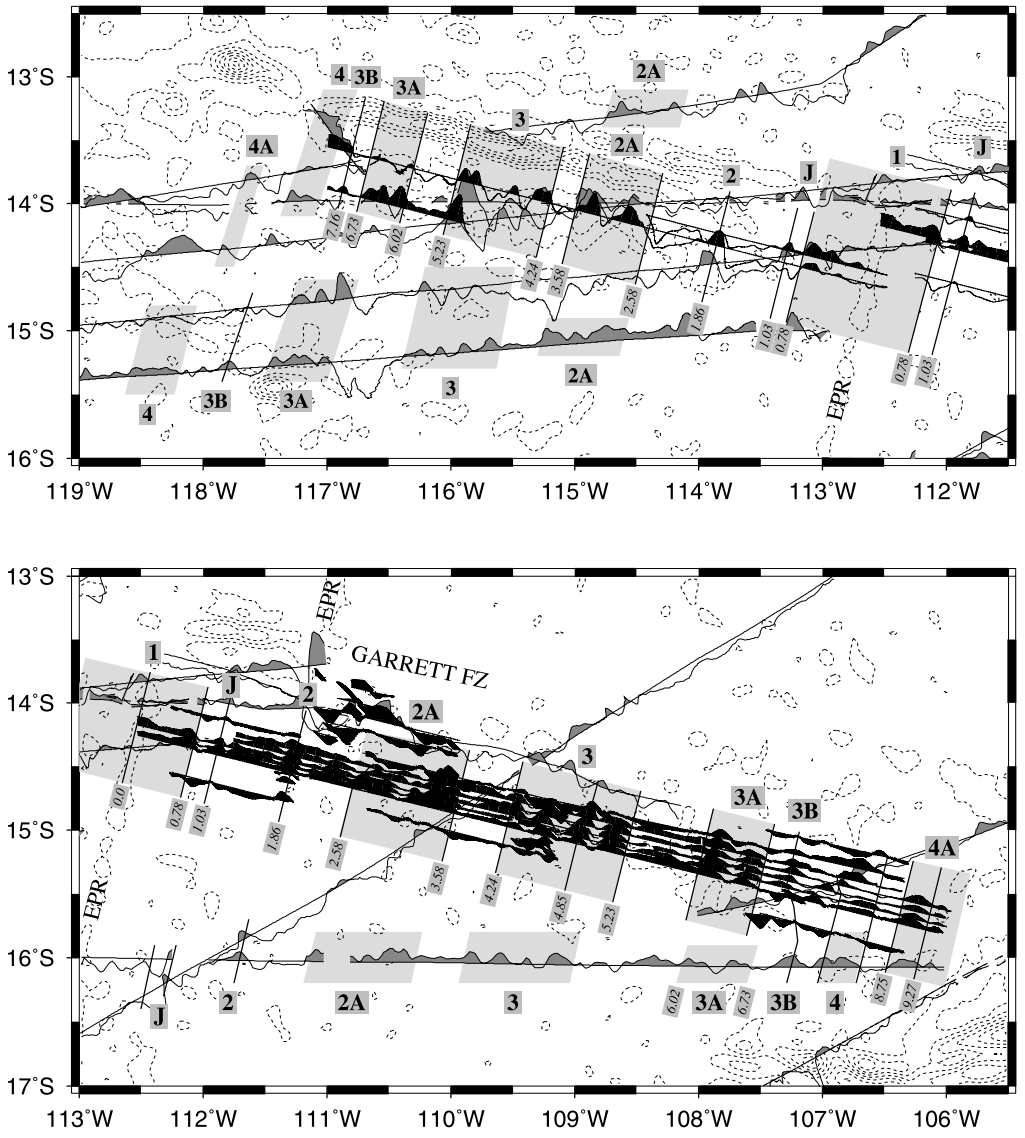

Fig. 2. Wiggle plot of magnetic data acquired on the East Pacific Rise south of the Garrett transform fault. Annotation above the surveyed corridors indicates the identified magnetic anomalies and numbers below give the seafloor age in million years [28–30]. Black wiggles are from the *Sonne* cruises and grey wiggles are from previous cruises. Isolines are gravity anomalies derived from satellite altimetry [5] (contour interval: 15 mGal).

tially interpreted by Grevemeyer et al. [13] who documented a correlation between changes in spreading rate and profound changes in the seafloor fabric as expressed by the rms height of abyssal hills. To verify whether these patterns are related to asymmetric spreading, a conjugate profile on the western flank was surveyed in 2000 during *Sonne* leg 145-1. However, because of the Sojourn Ridge [25] the profile had to be shifted by 30–40 km to the south. Additionally, the corridor on the eastern flank has been extended by flowline profiles to the north and south. Rock samples were dredged during *Sonne* leg 145-2 and provided basaltic lavas from 10 dredges on oceanic

crust and one dredge on a seamount. A further seven samples were recovered in the core catcher of a gravity corer.

3.1. Magnetics

Total magnetic field intensity was measured using a proton precession magnetometer. On the eastern flank up to seven flowline profiles allow an unambiguous identification of the sequence of reversals; coverage reaches 710 km off-axis. On the western flank only two profiles are available out to ~500 km in the spreading direction. For each survey the appropriate International Geomagnetic Reference Field (IGRF), which describes the long wavelength magnetic field for 5 yr intervals, has been removed from the observed magnetic field data. Unfortunately, the survey area is located close to the magnetic equator where daily variations are reasonably high [26]. We therefore calculated synthetic Sq variations and removed those from the field data. In addition, we tried to assess magnetic storms by using the worldwide DST index. Variations were calculated and removed. This procedure provided crossover errors for the corrected data, which are generally smaller than 25 nT [27]. In addition, we included magnetic tracks collected previously to our cruises to further constrain the spreading rate to the west and to the south of the survey area. The top and bottom panels of Fig. 2 show wiggle plots of the residual magnetic anomaly. Geomagnetic polarity reversals of Cande and Kent [28] were generally used to derive the crustal age. However, ages of anomaly #C3A and anomalies #C3B to #C4A are from Krijgsman et al. [29] and Hilgen et al. [30], respectively. The oldest anomaly on the western flank is #C4A (8.75 Ma) at 533 km off-axis and on the eastern flank #C4Ar1 (9.27 Ma) at 708 km off-axis. In Fig. 3 the age of the identified magnetic anomalies is plotted as a function of offset from the ridge axis, hence showing the half spreading rate.

3.2. Bathymetry

The multibeam-sonar data are from a HY-

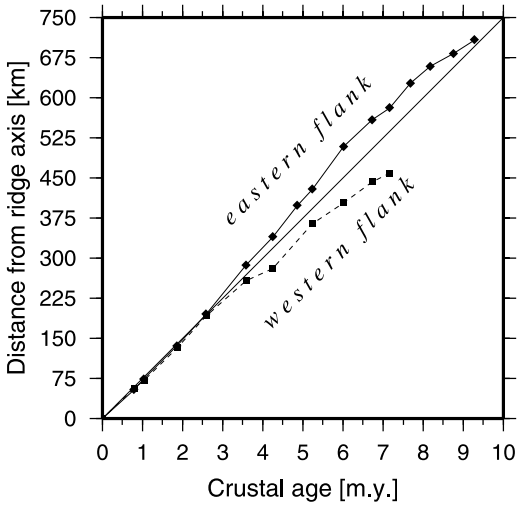

Fig. 3. Distance versus age plot of the picked magnetic reversals for the eastern and western ridge flank. The straight line indicates a half spreading rate of 75 mm/yr; thus, before 2.7 Ma seafloor spreading was asymmetric with faster spreading to the east.

DROSWEEP swathmapping echosounder [31]. The 59 beams fired within an angle of 90° survey a stripe on the seabed with a width about twice the water depth. These data have been processed and edited with the MB Software from the Lamont-Doherty Earth Observatory [32]. The resulting digital terrain models (DTM) were displayed and imaged with the GMT Software [33]. In total, about 15 000 line km of swath bathymetry covered about 35 000 km^2 of seafloor. On the eastern flank nearly full coverage extends up to 720 km off-axis. The width of the corridor is between 50 and 80 km. Detailed maps are shown in Fig. 4.

3.3. Geochemical analytical methods

The geochemistry study is based on investigations carried out on more than 50 samples of mid-ocean ridge basalt (MORB) from 17 locations. Sample locations are shown in Fig. 4 and mean major element compositions are summarized in Table 1. The samples were recovered either by dredging or in the core catcher of a gravity corer. Major element analyses were carried out on a five

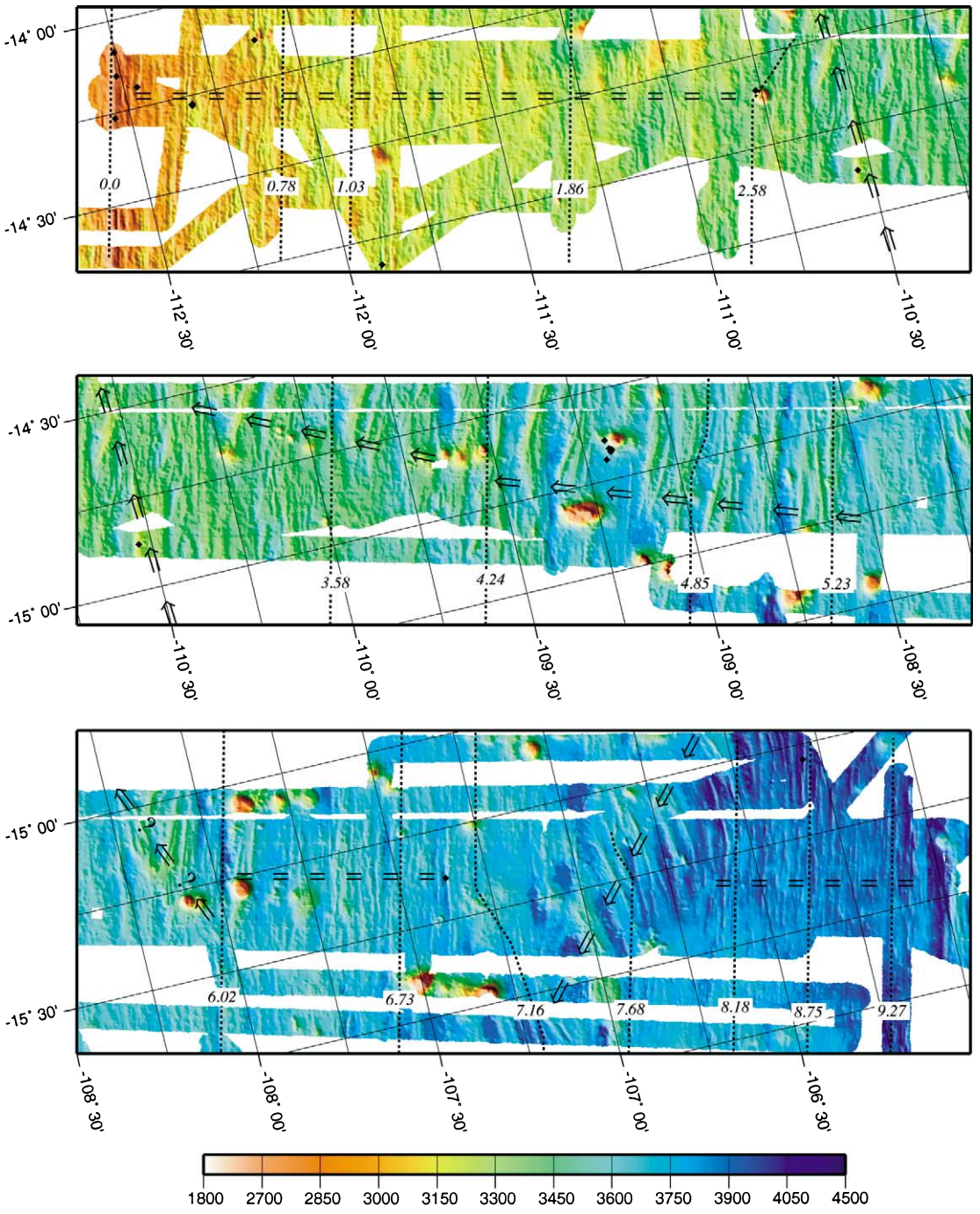

Fig. 4. Oblique projection of the bathymetry derived from the multibeam-sonar data. Data are displayed with artificial illumination. Seafloor fabric which plot vertically in the figure runs parallel to the strike of the ridge crest. Hummocky basins and motley texture of curved lineations striking oblique to the ridge axis are caused by at least five migration events of overlapping spreading centres. Broken horizontal lines mark times characterized by stable spreading condition at the ridge crest. Arrows show the migration paths of non-transform ridge axis discontinuities. Dotted lines are chrons in million years. Sample locations are shown by diamonds.

Table 1
Average microprobe analyses of glassy MORB pieces from *Sonne* leg 145-2 (wt%)

Sample	Ma	Latitude	Longitude	Eruption latitude	SiO_2	TiO_2	Al_2O_3	FeO	MnO	MgO	CaO	Na_2O	K_2O	P_2O_5	Cr_2O_3	Total	*n*	Mg#
21DS all	0.000	−14°05	−112°30	−14.086	50.64	1.80	14.36	10.69	0.20	7.51	11.63	2.98	0.13	0.15	0.04	100.13	70	0.56
18DS all	0.015	−14°16	−112°33	−14.264	50.63	1.85	13.86	11.35	0.20	7.25	11.32	2.90	0.13	0.14	0.03	99.66	54	0.53
20DS rest	0.015	−14°09	−112°31	−14.154	50.58	1.68	14.04	10.97	0.20	7.52	11.65	2.69	0.11	0.12	0.04	99.58	21	0.55
20DS3	0.015	−14°09	−112°31	−14.154	49.88	1.68	14.71	10.29	0.18	7.63	11.79	2.83	0.19	0.15	0.05	99.39	5	0.55
22DS all	0.120	−14°12	−112°28	−14.167	49.50	2.16	13.09	11.97	0.21	6.77	10.87	2.71	0.11	0.19	0.02	97.60	83	0.50
27SL all	0.360	−14°17	−112°19	−14.216	50.04	2.03	13.63	11.75	0.22	6.88	11.01	2.77	0.12	0.16	0.02	98.63	37	0.51
15SL rest	0.360	−14°16	−112°19	−14.215	50.50	2.16	13.54	12.30	0.23	6.78	11.00	2.80	0.14	0.15	0.02	99.61	7	0.50
15SL3	0.360	−14°16	−112°19	−14.215	50.09	1.33	13.94	10.24	0.20	7.66	12.07	2.55	0.02	0.09	0.03	98.23	10	0.57
26SL all	0.360	−14°17	−112°19	−14.219	49.50	1.67	13.98	10.21	0.20	7.38	11.37	2.73	0.09	0.16	0.04	97.33	22	0.56
28DS all	0.650	−14°09	−112°07	−14.026	49.00	0.92	16.68	9.59	0.18	10.09	11.57	2.16	0.09	0.06	0.06	100.40	49	0.65
29DS rest	1.160	−14°49	−111°54	−14.632	50.46	2.23	13.78	11.94	0.21	6.72	11.04	3.06	0.20	0.21	0.02	99.87	30	0.50
29DSE	1.160	−14°49	−111°54	−14.632	53.86	1.92	13.30	12.16	0.22	4.84	8.84	3.54	0.36	0.37	0.02	99.43	20	0.41
35DS all	2.560	−14°36	−110°46	−14.167	50.13	1.17	15.13	9.46	0.17	8.54	12.77	2.38	0.04	0.06	0.05	99.91	9	0.62
9DS rest	2.920	−14°52	−110°32	−14.389	49.84	2.79	12.68	14.57	0.25	5.72	9.83	3.15	0.19	0.24	0.01	99.27	18	0.41
9DS4	2.920	−14°52	−110°32	−14.389	49.83	2.23	13.70	11.97	0.21	6.84	11.04	2.97	0.17	0.18	0.04	99.17	9	0.50
9DS8	2.920	−14°52	−110°32	−14.389	49.67	1.64	14.92	10.05	0.18	7.68	11.98	2.96	0.15	0.13	0.06	99.42	10	0.58
37SL rest	4.590	−14°57	−109°12	−14.143	49.96	1.39	13.92	10.47	0.20	7.85	12.18	2.61	0.04	0.09	0.03	98.71	14	0.57
37SL1	4.600	−14°57	−109°12	−14.143	49.51	1.01	15.28	8.87	0.17	8.82	12.56	2.30	0.02	0.07	0.06	98.66	22	0.64
36DS all	4.600	−14°54	−109°11	−14.108	49.58	1.09	15.61	9.35	0.17	9.09	12.67	2.45	0.04	0.06	0.07	100.16	7	0.63
38SL all	4.610	−14°55	−109°11	−14.121	50.24	1.24	14.41	9.91	0.19	8.03	12.42	2.65	0.02	0.07	0.03	99.21	41	0.59
40SL rest	4.610	−14°56	−109°11	−14.130	49.17	1.02	15.49	8.94	0.16	8.94	12.61	2.33	0.02	0.06	0.06	98.81	27	0.64
40SL3	4.610	−14°56	−109°11	−14.130	49.87	2.09	13.23	11.92	0.22	6.63	10.62	2.78	0.11	0.18	0.03	97.68	13	0.50
7SL1+3	4.620	−14°55	−109°10	−14.162	49.34	1.00	15.23	8.88	0.17	8.87	12.52	2.33	0.02	0.05	0.06	98.45	13	0.64
7SL2+3	4.620	−14°55	−109°10	−14.162	49.94	1.21	14.20	10.02	0.19	7.82	12.34	2.58	0.02	0.08	0.04	98.43	17	0.58
42DS all	6.840	−15°23	−107°22	−14.189	50.03	1.94	13.85	11.57	0.21	7.12	11.43	2.83	0.13	0.15	0.03	99.28	17	0.52
43DS all	8.640	−15°18	−106°18	−13.895	50.52	1.91	14.09	10.99	0.20	7.45	11.59	2.81	0.11	0.14	0.03	99.85	17	0.55
	Analytical error (1 S.D. relative %)				*0.64*	*3.70*	*1.17*	*1.57*	*9.22*	*1.80*	*1.23*	*3.20*	*23.82*	*24.80*	*59.39*	*0.48*		*0.87*

Averages are either of single samples (in the cases where the letters in the sample names are followed by numbers) or of many or all samples from a dredge haul (shown by the word rest or all in the sample names). Sample 22DS is an analysis of bulk rock powder fused to a glass. Eruption latitude is discussed in the text; *n*, number of analyses used to build the mean. The age of the samples was derived by linear interpolation between the age of magnetic reversals (Fig. 2).

Table 2
Summary of results and interpretation of seafloor fabric generated at the EPR near 14°14′S over the last 10 Myr

Time interval	Magnetic lineations	Strike of seafloor fabric	Advance of discordant zones	Interpretation
0.0–2.5 Ma	ridge parallel	013°	none	stable system
2.5–~2.7 Ma	right lateral offset by 20–30 km	oblique, curving SW	northward	northward migrating right-stepping OSC
~2.7–4.2 Ma	ridge parallel	oblique, curving SW	slowly northward	slowly northward migrating right-stepping OSC
4.2–5.3 Ma	right lateral offset	oblique, curving SW, fossil overlap basin	none?	duelling OSC
5.3–5.5 Ma	–	smooth seafloor	–	stable system
5.5–6.0 Ma	–	oblique, curving SW	northward	northward migrating right-stepping OSC
6.0–7.2 Ma	ridge parallel	013°	none	stable system
7.2–~7.8 Ma	left lateral offset by 20–30 km	oblique, curving NW	southward	southward migrating left-stepping OSC
~7.8–~9.4 Ma	ridge parallel	013°	none	stable system

spectrometer JEOL JXA 8900 RL electron microprobe (University of Göttingen, Germany) either on natural glass pieces from pillow rinds or, in the case of sample 22DS, on glasses produced by melting powdered groundmass on a platinum wire in the laboratory. Analytical conditions were 15 kV accelerating voltage and 11–13 nA sample current. Representative errors on the analyses are shown in Table 1 together with the number of individual spots measured and used to calculate the mean values. The electron beam was slightly defocused (10 μm diameter) to avoid the volatilization of alkalis. The raw major element data from each measured spot have been corrected to the KL2-G MPI-DING reference glass [34]. We note that the samples from the gravity corer (samples labelled SL) and from the melted powdered groundmass (22DS) have analytical totals lower than the acceptable 99.6 ± 0.5% found for all other samples. We attribute this to hydration of the glasses in the case of gravity corer samples and to the inclusions of microbubbles of air during the melting of the powder in the case of 22DS. We do not expect either of these effects to alter the Mg/Fe ratio of the measurement; their effects are therefore unimportant for the conclusions of the paper.

4. Results and discussion

4.1. Asymmetric spreading and segmentation

Since 10 Ma, seafloor spreading rates derived from the magnetic data indicate an average total separation rate of the Nazca plate and Pacific plate of 150 mm/yr (Fig. 3), which is in reasonable agreement with the NUVEL-1A spreading model of current plate motions [18]. However, symmetric spreading has occurred only since about 3 Ma. In Early Pliocene and Late Miocene times the spreading rate was profoundly asymmetric. In general, faster spreading rates of the Nazca plate to the east of the rise axis are compensated by slower spreading rates of the Pacific plate to the west. It is important to note that magnetic data immediately to the south of the survey corridor show a right-lateral offset of the magnetic spreading anomalies on both ridge flanks. Unfortunately, these profiles do not follow the flowline. Nonetheless, they clearly suggest that spreading was asymmetric and faster to the east. However, this asymmetry is not as pronounced as immediately to the north.

In a statistical study of seafloor fabric Grevemeyer et al. [13] show a change in seafloor fea-

tures at about 225 km off-axis. This offset corresponds to the 3 Ma isochron derived from the magnetic data. The high-resolution bathymetric maps in Fig. 4 show that within 225 km of the rise axis (out to about 110°45′S) abyssal hills strike parallel to the ridge axis and therefore imply a spreading system similar to the present configuration of the ridge at 14°14′S. Beyond 110°45′W, however, the seafloor fabric is orientated obliquely to the 013° strike of the ridge axis. In addition, the magnetic anomaly #C2ay (2.58 Ma) indicates a right-lateral offset of 20–30 km. Such features are generally taken as evidence for off-axis discordant zones of migrating OSC [4,19,21]. This interpretation is supported by bathymetric studies within the adjacent MELT study area. Immediately to the south, Cormier et al. [25] found similar features, which they interpreted as the trace of a right-stepping northward migrating OSC.

East of 110°20′W the surveyed corridor indicates a wedge of rough terrain in the northern part of the swath. This zone is comprised of hummocky basins and motley lineaments, interpreted as abandoned curvilinear ridge tips of OSCs. In terms of Wilson's [35] model for overlapping rift propagation, we would interpret the curvature and the trace of the discordant zone (or inner pseudofault) to result from a right-stepping northward migrating OSC. This idea is supported by a right-stepping offset of the magnetic anomaly #C3.3 (4.85 Ma) and seafloor younger than anomaly #C3.1 (4.24 Ma) indicates a northward shift of the discordant zone. Other features resemble fossil overlap basins, for example the seafloor fabric near 109°20′W. Nonetheless, features are not consistent; the curved abandoned tips between anomaly #C3.3 (4.85 Ma) and #C3o (5.23 Ma) seem to indicate only a small or no northward shift. Unfortunately, seafloor coverage is not complete. However, to explain the seafloor fabric we propose a model including a northward migrating right-stepping OSC, which was active between ~2.7 Ma and 4.24 Ma; features between chron ~4.24 and ~5.3 Ma are interpreted to result from a right-stepping duelling OSC.

Immediately to the east of 108°30′W the seafloor is very smooth for about 30 km. Features between 108°15′W and 108°00′W are not very clear. Some structural elements, such as the curvature of abyssal hills, may indicate a northward migrating right-stepping OSC. However, the magnetic anomaly #C3Ay (6.02 Ma) does not indicate any right-lateral step.

East of chron 6.02 Ma the seafloor is smooth and the abyssal hill fabric strikes parallel to the present trend of the ridge axis until magnetic anomaly #C3B (7.16 Ma) is reached. This suggests a stable spreading regime similar to the present situation at 14°14′S. Nevertheless, to the north and south several large seamounts have been surveyed. Swathmapping data suggest, however, that seamount volcanism on the eastern ridge flank at 14°14′S has been relatively scarce during the last 3 Myr.

The ridge axis was offset by another OSC between 107°15′W and 106°45′W. The orientation of abandoned ridge tips indicates a left-stepping OSC. This fact is supported by the magnetic data, which indicate a left-lateral offset of 20–30 km of anomaly #C4n.1r (7.68 Ma). In addition, the seafloor fabric shows an inner pseudofault and suggests that the OSC migrated southward. This fact is important to note and will be discussed below.

At the end of the survey area, i.e., east of 106°40′W, the seafloor is remarkably smooth. Additionally, the swathmapping revealed no seamounts. Seafloor in this area is between ~7.8 and ~9.4 Ma and may have been formed by a crustal accretion process similar to that typical for the rise axis since ~3 Ma.

A summary of the Late Miocene to Pleistocene segmentation of the SEPR at 14°14′S is given in Table 2. The features detected in the seafloor fabric provide a reasonable explanation for the degree of asymmetric spreading detected in the magnetic data. Both northward migrating right-stepping and southward migrating left-stepping overlapping spreading centres transfer lithosphere from the Pacific plate to the Nazca plate and may therefore account for the spreading asymmetry. With respect to previous studies of the ridge flanks immediately to the south [19,21], it seems reasonable to suggest that between the Garrett fracture zone and the OSC at 20°40′S the majority of the spreading asymmetry is accommodated

by migrating OSC. Immediately to the south of the detailed study area our interpretation of magnetic tracks (Fig. 2) suggests a less prominent degree of asymmetric spreading. On the western flank, about two degrees to the south, magnetic anomaly #C4n.1r was identified approximately 580 km away from the ridge crest. Back tracking of the anomaly suggests that this crust was created where the SEPR intersected latitude 16°S. Its distance from the ridge axis indicates a spreading half rate of about 75 mm/yr, which is exactly the rate predicted by the NUVEL-1A spreading model [18]. Consequently, the existing data may argue that the spreading asymmetry observed at 14°14′S is a local feature primarily related to the tectonic evolution of the rise axis north of 16°S. However, the identification of the magnetic anomalies south of the flowline corridor may not be entirely reliable. Therefore, additional profiles will be necessary to constrain the tectonic evolution of the 14.5°S to 16°S area between 5 and 10 Ma.

4.2. Tectonic and geochemical segmentation

The underlying principle of ridge segmentation presented by Macdonald et al. [3] is the along axis migration of melt away from the shallowest portions of the rise axis which coincide with localized regions of asthenospheric upwelling. Thus, gravitational spreading forces due to excess ridge topography cause a segment to lengthen and force a discontinuity to migrate [36]. Because magma supply beneath the ridge axis will tend to be enhanced over loci of partial melting in the upper mantle, this model works well where hot spot magmatism has produced extraordinary ridge axis elevation and significant variations in near-field stresses. It may also work if focused mantle upwelling occurs [37]. However, at ~7.3–7.8 Ma a southward migrating OSC dominated the rise axis at 14°14′S and must have originated close to the Garrett transform fault. Although the primary segmentation of the southern EPR around ~8 Ma is largely unconstrained, work of Goff and Cochran [38] suggest that the Garrett transform already offset the EPR between 8 and 10 Ma. Near first-order discontinuities, a small cross-sectional area and a deepening of the ridge crest towards the transform fault is generally interpreted as evidence for a starved magma supply at the ends of a spreading segment [8]. Consequently, an OSC migrating away from a transform fault is inconsistent with a model where the migration of non-transform ridge axis discontinuities is controlled by the along axis distribution of melt. In addition, the few existing magnetic profiles to the south of the detailed study area suggest a less prominent degree of asymmetric spreading near 16°S, which makes it unlikely that all of the detected OSCs have been created in the middle of the first-order segment near 18–19°S, but instead somewhere north of 16°S. Therefore, forces other than mantle upwelling and melting may control the creation and migration of overlapping spreading centres.

Wilson et al. [39] proposed a model which suggested that migration events of non-transform ridge axis discontinuities are caused by far-field stresses related to the reorientation of a plate boundary and Macdonald et al. [4] suggested that crack propagation caused by such far-field stresses might cause discontinuities to migrate. Such models appeal to us because they may explain how an OSC can originate close to a magmatically starved first-order discontinuity. Following the breakup of the Farallon plate a major reorientation of the plate boundary configuration occurred in the southern East Pacific Ocean about 20 Myr ago and included the formation of the Bauer microplate [20,38]. Goff and Cochran [38] investigated the evolution of the Bauer microplate and a now extinct spreading ridge: the Galapagos Rise. Between ~17 and ~6 Ma two spreading centres were active between latitudes ~2°S and ~16°S. Because the Galapagos Rise was orientated obliquely to the EPR, it is reasonable to assume that the resulting stress field affected the on-axis stress field of the southern EPR and perhaps forced the migration of the OSC. Therefore, the southward migrating OSC, which was generated at or near the Garrett transform fault, was perhaps forced by far-field stresses caused by the plate boundary reorientation and evolution of the Bauer microplate. In addition, back tracking of the OSCs dominating the SEPR at 14°14′S between magnetic chron #C3.1

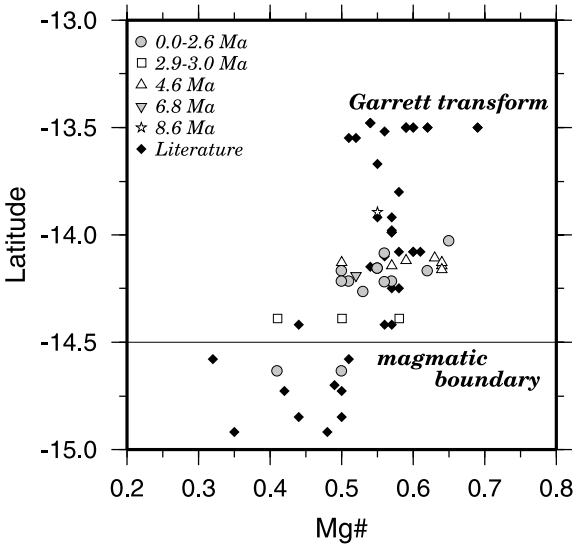

Fig. 5. Geochemical data (Mg#) back tracked to the ridge crest. The common trend of samples (labelled literature) from the ridge crest [10,40,41] and off-axis samples argues that the latitudinal variations in magma composition are a robust feature of the sub-lithospheric magmatic system and independent of the shallow processes controlling the propagation of non-transform ridge axis discontinuities.

(4.24 Ma) and #C3Ay (6.02 Ma) points toward the fossil Bauer fracture zone (Fig. 2, gravity anomaly in the lower right hand corner), which marked the southern terminus of the Bauer microplate [38]. The birth of both OSCs was probably related to a change of the regional stress pattern as spreading at the Galapagos Rise ceased and the EPR-Bauer-microplate ridge-ridge-transform triple junction became inactive ~6 Ma ago.

Additional support for a crack model rather than a melt migration model is provided by the geochemical data from the seafloor samples. The works of Langmuir et al. [1] and Sinton et al. [10] suggest that the tectonic and chemical segment boundaries are linked. They suggest that all first-, second- and third-order ridge offsets correspond to secondary magmatic segment boundaries, although some secondary magmatic boundaries may even occur at small, fourth-order discontinuities. Secondary magmatic segments are believed to define the length scale of mantle melting variations, which are mainly variations in extent of melting, but are not necessarily the scale of melt extraction processes that feed the axis. Melt extraction is suggested to correspond to the length scale of fourth-order physical segments [10]. The samples collected on the eastern flank are sparse but still define an important dataset, because they provide the means to study temporal variations in magma geochemistry. In this paper, we report only some initial results of the geochemistry. In Fig. 5, all samples have been projected back to their eruption latitude and plotted together with data from samples taken on the present day axis [10,40,41]. A striking feature of the present day axis is a significant and systematic variation of Mg# with latitude, characterized by high Mg# of about 0.6 for lavas north of a DEVAL at 14°30′S. South of this DEVAL all magmas show Mg# lower than ca. 0.5. In general, Sinton et al. [10] found that most secondary magmatic boundaries defined by K/Ti and K/P ratios correspond to boundaries apparent in MgO content. The prominent Mg# boundary at 14°30′S, however, occurred within a secondary magmatic segment and hence defines a tertiary magmatic and fourth-order physical segment boundary. Sinton et al. [10] attributed this type of magmatic segmentation to mixture boundaries within the continuous magma chambers. Therefore, it is surprising that the back tracked data show exactly the same patterns of Mg# variations with latitude, despite the fact that they cover a range of ages back to ca. 10 Ma. The bathymetric data clearly show that up to five OSCs dominated the ridge morphology for various amounts of time in the period 2.6–7.8 Ma. In total, we have sampled six locations from two sites affected by OSCs and 14 locations (including one on-axis and three at ~15 ka) from sites, which, based on the bathymetric data, were characterized by stable spreading conditions similar to those of the present day (Fig. 4). Unfortunately, only one dredge provided two samples to the south of the 14°30′S magmatic boundary on 1 Myr old crust. Nevertheless, DEVALs are generally believed to last only for 10^2–10^4 yr [8]; thus, it is remarkable that its geochemical signature lasted for at least 1 Myr and maybe even longer. Because all the data from our survey, irrespective of tectonic setting, plot within the Mg# vs. Latitude trend seen at the present day

on the axis, we believe that magmatic segmentation defined by the change in Mg# at 14°30′S has been stationary over the last ~10 Myr.

In an overview of the East Pacific Rise morphology, Macdonald [8] quantified the commonly noted observations that primitive basalts tend to be found on the shallower and broader parts of the ridge axis and emphasized the 14°30′S discontinuity as a place where basalt chemistry correlates much better with cross-sectional area of the ridge axis than with simple axial depth. The more evolved lavas to the south are associated with a cross-section of 3–4 km^2, while the more primitive lavas to the north are associated with an area of 4–5 km^2. Axial depth is nearly uniform at 2620–2660 m. If the chemical discontinuity has been persistent, as we suggest, then one speculative interpretation is that the broad cross-section reflects an extremely stable and robust site of upwelling that has neither influenced nor been influenced by small ridge offsets that have propagated through the area. Although the causes of variation in magma fractionation along ridge axes remain poorly understood, it is widely accepted that frequent replenishment of shallow crustal magma chambers would generally dilute any evolved magmas that may form there.

We conceive of two plausible mechanisms to explain the observation of a stationary chemical segmentation defined by Mg#. Either (1) the magmas being supplied from the mantle have similar Mg# over the whole area and the extent of crystal fractionation occurring in the sub-axial magma chamber is consistently higher (and by implication the rate of magma supply consistently lower [10]) towards the south of the 14°30′S discontinuity or (2) the Mg# of the parental magmas decreases systematically southward and the extent of fractionation stays constant. In view of the fact that total crustal thickness (as indicated by axial depths) appears to be constant over the area, the former option would imply a systematic change in the Layer 2/Layer 3 thickness from north to south (assuming that Layer 3 represents the cumulates and Layer 2 the residual liquids from fractionation). Data from Hooft et al. [9] show constant Layer 2A thickness throughout the region studied here and appear to provide some evidence against changing extents of crystal fractionation. We therefore must conclude that the latitudinal variations in magma composition are principally a feature of the sub-lithospheric magma supply and relatively independent of crustal processes.

The fact that the composition of the lavas between the Garrett transform and 14°30′S appears to remain constant over the last 10 Myr and the lack of correlation of compositional boundaries with off-axis discordant zones provide important implications for the processes controlling the segmentation of mid-ocean ridges. We propose that these observations provide further support for a crack model. As a cracking front advances along the ridge axis, it is likely to intersect and tap a number of separate mantle melt sources. Magmas would rise passively into the open crack and erupt on the seafloor. Thus, such a model would be dominantly plate- and crack-controlled and hence a passive spreading model. Nevertheless, focused mantle upwelling [37] would result in an increased melt supply toward the middle of a first-order segment and in the presence of magma, crustal failure can occur at much lower deviatoric stresses [42]. It therefore seems likely that overlapping spreading centres will generally tend to originate near the middle of a first-order segment and may support a feedback between passive and active driving forces, as proposed by Macdonald et al. [4]. However, four out of five OSCs imaged in our dataset are probably linked to far-field stresses related to the evolution of the now extinct Bauer microplate and originated somewhere near 16°S and hence well to the north of the middle of the first-order segment.

5. Conclusions

A combined geophysical mapping and geochemical sampling approach provided a unique dataset from a flowline corridor out to a seafloor age of ~10 Ma on the eastern flank of the East Pacific Rise at 14°14′S. In addition to multibeam-sonar data and magnetic anomalies from the eastern flank, magnetic and bathymetric data were obtained on the conjugate western flank to esti-

mate the degree of asymmetric spreading. Seafloor spreading was generally asymmetric with a faster spreading to the east, although since ~2.8 Ma crustal accretion occurs symmetrically. The seafloor characterized by symmetric spreading did not show any evidence for discordant zones, while seafloor indicating asymmetric spreading suffered from at least five overlapping spreading centre migration events. One was a left-stepping southward migrating discontinuity, which was created close to the Garrett transform fault. The other four were right-stepping and northward migrating OSCs and originated somewhere near 16°S. Both right-stepping northward and left-stepping southward migrating OSC transfer lithosphere from the Pacific plate to the Nazca plate and may therefore account for the spreading asymmetry. The fact that the birth of four of the five OSCs seems to be initially related to the evolution of the Bauer microplate between ~9 and 6 Ma suggests that in addition to mantle upwelling other forces – like far-field stresses – can create non-transform ridge axis discontinuities. Furthermore, the geochemical data seem to support a crack-controlled rather than upwelling-controlled model for higher-order ridge crest segmentation. They suggest that the magmatic segment boundary near 14°30′S has remained stationary for at least the last 10 Myr. Moreover, the geochemistry of samples does not show any correlation with off-axis discordant zones of fossil OSCs. This observation suggests that advancing cracks tap underlying melt reservoirs and melts rise passively into the crack to build the seafloor. Thus, to explain all observations we favour a feedback mechanism between active and passive plate- and crack-controlled spreading mechanisms. Magma, however, is not distributed along axis by propagating segment tips.

Acknowledgements

We are grateful to Milene Cormier, Jennifer Reynolds and Maurice Tivey for their reviews, which led to substantial improvements in the manuscript. This work was supported by the German Ministry of Education, Science, Research and Technology (grants 03G0105A and 03G0145A). We would particularly like to thank the masters, crews and shipboard scientific parties of research vessel *Sonne* cruises 105 and 145 for their efficiency and cooperation at sea. *[AC]*

References

[1] C.H. Langmuir, J.F. Bender, R. Batiza, Petrological segmentation of the East Pacific Rise, 5°30′-14°30′N, Nature 322 (1986) 422–429.
[2] H. Schouten, K.D. Klitgord, J.A. Whitehead, Segmentation of mid-ocean ridges, Nature 317 (1985) 225–229.
[3] K.C. Macdonald, P.J. Fox, L.J. Perram, M.F. Eisen, R.M. Haymon, S.P. Miller, S.M. Carbotte, M.-H. Cormier, A.N. Shor, A new view of the mid-ocean ridge from the behaviour of ridge axis discontinuities, Nature 335 (1988) 217–225.
[4] K.C. Macdonald, D.S. Scheirer, S.M. Carbotte, Mid-ocean ridges: discontinuities, segments and giant cracks, Science 253 (1991) 986–994.
[5] D.T. Sandwell, W.H.F. Smith, Marine gravity anomaly from Geosat and ERS-1 satellite altimetry, J. Geophys. Res. 102 (1997) 10039–10054.
[6] B.E. Tucholke, J. Lin, M.C. Kleinrock, M.A. Tivey, T.B. Reed, J. Goff, G.E. Jaroslow, Segmentation and crustal structure of the western Mid-Atlantic Ridge flank, 25°25′–27°10′N and 0–29 m.y., J. Geophys. Res. 102 (1997) 10203–10223.
[7] D.S. Scheirer, K.C. Macdonald, D.W. Forsyth, S.P. Miller, D.J. Wright, M.-H. Cormier, C.M. Weiland, A map series of the southern East Pacific Rise and its flanks, Mar. Geophys. Res. 18 (1996) 1–12.
[8] K.C. Macdonald, Linkages between faulting, volcanism, hydrothermal activity and segmentation on fast spreading centers, in: W.R. Buck, P.T. Delaney, J.A. Karson, Y. Lagabrielle (Eds.), Faulting and Magmatism at Mid-Ocean Ridges, Geophys. Monogr. 106 (1998) 27–58.
[9] E.E.E. Hooft, R.S. Detrick, G.M. Kent, Seismic structure and indicators of magma budget along the Southern East Pacific Rise, J. Geophys. Res. 102 (1997) 27319–27340.
[10] J.M. Sinton, S.M. Smaglik, J.J. Mahoney, K.C. Macdonald, Magmatic processes at the superfast spreading mid-ocean ridges: glass compositional variations along the East Pacific Rise 13°–23°S, J. Geophys. Res. 96 (1991) 6133–6155.
[11] J.-C. Sempéré, K.C. Macdonald, Overlapping spreading centers: implications from crack growth simulation by the displacement discontinuity methods, Tectonics 5 (1986) 151–163.
[12] W. Weigel, I. Grevemeyer, N. Kaul, H. Villinger, T. Lüdmann, H.K. Wong, Aging of oceanic crust at the southern East Pacific Rise, EOS Trans. Am. Geophys. Un. 77 (1996) 504.

[13] I. Grevemeyer, V. Renard, C. Jennrich, W. Weigel, Seamount abundances and abyssal hill morphology on the eastern flank of the East Pacific Rise at 14°S, Geophys. Res. Lett. 24 (1997) 1955–1958.
[14] I. Grevemeyer, N. Kaul, H. Villinger, W. Weigel, Hydrothermal activity and the evolution of the seismic properties of upper oceanic crust, J. Geophys. Res. 104 (1999) 5069–5079.
[15] C.W. Devey, H. Villinger, I. Grevemeyer, J. Hauschild, K. Lackschewitz, N. Kaul, M. Mottl, M. Pfender, B. Schramm, G. Wheat, and scientific party EXCOII legs 1 and 2, The fourth dimension in ridge studies: sampling along a flow-line corridor 0–9 Ma at 14°S on the EPR, InterRidge News 9 (2000) 34–36.
[16] R.S. Detrick, A.J. Harding, G.M. Kent, J.A. Orcutt, J.C. Mutter, P. Buhl, Seismic structure of the southern East Pacific Rise, Science 259 (1993) 499–503.
[17] G.M. Kent, A.J. Harding, J.A. Orcutt, R.S. Detrick, J.C. Mutter, P. Buhl, Uniform accretion of oceanic crust south of the Garrett transform at 14°15′S on the East Pacific Rise, J. Geophys. Res. 99 (1994) 9097–9116.
[18] C. DeMets, R.G. Gordon, D.F. Argus, S. Stein, Effect of recent revisions to the Geomagnetic Reversal Time Scale on estimates of current plate motions, Geophys. Res. Lett. 21 (1994) 2191–2194.
[19] M.-H. Cormier, D.S. Scheirer, K.C. Macdonald, Evolution of the East Pacific Rise at 16°–19° S since 5 Ma: bisection of overlapping spreading centers by new, rapidly propagating segments, Mar. Geophys. Res. 18 (1996) 53–84.
[20] P. Lonsdale, Segmentation of the Pacific-Nazca spreading center, 1°N–20°S, J. Geophys. Res. 94 (1989) 12197–12225.
[21] M.-H. Cormier, K.C. Macdonald, East Pacific Rise 18°–19°S: asymmetric spreading and ridge reorientation by ultrafast migration of axial discontinuities, J. Geophys. Res. 99 (1994) 543–564.
[22] K.C. Macdonald, R.M. Haymon, S.P. Miller, J.-C. Sempéré, P.J. Fox, Deep-tow and SeaBeam studies of dueling propagating ridges on the East Pacific Rise near 20°40′S, J. Geophys. Res. 93 (1988) 2875–2898.
[23] L.J. Perram, M.-H. Cormier, K.C. Macdonald, Magnetic and tectonic studies of the dueling propagating spreading centers at 20°40′S on the East Pacific Rise: evidence for crustal rotations, J. Geophys. Res. 98 (1993) 13835–13850.
[24] I. Grevemeyer, W. Weigel, C. Jennrich, Structure and ageing of oceanic crust at 14°S on the East Pacific Rise, Geophys. J. Int. 135 (1998) 573–584.
[25] M.-H. Cormier, D.S. Scheirer, K.C. Macdonald, S. White, R.M. Haymon, and the Sojourn Leg 1 Scientific Party, Sojourn, Leg 1: detailed study of the asymmetries about the East Pacific Rise, 15°30′–20′S, Ridge Events 8 (1997) 1–5.
[26] A.P. Hitchman, F.E.M. Lilley, W.H. Campbell, The quite daily variation in the total magnetic field: global curves, Geophys. Res. Lett. 25 (1998) 2007–2010.
[27] B. Jochum, Geomagnetische Untersuchungen am Ostpazifischen Rücken unter Benutzung simulierter magnetischer Variationen, M.Sc. thesis, Inst. Meteorology and Geophysics, Univ. Vienna, Vienna, 1996, 70 pp.
[28] S.C. Cande, D.V. Kent, Revised calibration of the geomagnetic polarity timescale for the Late Cretaceous and Cenozoic, J. Geophys. Res. 100 (1995) 6093–6095.
[29] W. Krijgsman, F.J. Hilgen, I. Raffi, F.J. Sierro, D.S. Wilson, Chronology, causes and progression of the Messinian salinity crisis, Nature 400 (1999) 652–655.
[30] F.J. Hilgen, W. Krijgsman, C.G. Langereis, L.J. Lourens, A. Santarelli, W.J. Zachariasse, Extending the astronomical (polarity) time scale into the Miocene, Earth Planet. Sci. Lett. 136 (1995) 495–510.
[31] J.A. Grant, R. Schreiber, Modern swathe sounding and sub-bottom profiling technology for research applications: the Atlas Hydrosweep and Parasound systems, Mar. Geophys. Res. 12 (1990) 9–19.
[32] D.W. Caress, D.N. Chayes, Improved processing of Hydrosweep DS multibeam data on the R/V Maurice Ewing, Mar. Geophys. Res. 18 (1996) 631–650.
[33] P. Wessel, W.H.F. Smith, Free software helps map and display data, EOS Trans. Am. Geophys. Un. 72 (1991) 441, 445–446.
[34] K.P. Jochum, D.B. Dingwell, A. Rocholl, B. Stoll, A.W. Hofmann, The preparation and preliminary characterisation of eight geological MPI-DING reference glasses for in-situ microanalysis, Geostand. Newslett. 24 (2000) 87–133.
[35] D.S. Wilson, Kinematics of overlapping rift propagation with cyclic rift failure, Earth Planet. Sci. Lett. 96 (1990) 384–392.
[36] J. Phipps Morgan, E.M. Parmentier, Causes and rate-limiting mechanisms of ridge propagation: a fracture mechanics model, J. Geophys. Res. 90 (1985) 8603–8612.
[37] J. Lin, J. Phipps Morgan, The spreading rate dependence of three-dimensional mid-ocean ridge gravity structure, Geophys. Res. Lett. 19 (1992) 13–16.
[38] J.A. Goff, J.R. Cochran, The Bauer scarp ridge jump: a complex tectonic sequence revealed in satellite altimetry, Earth Planet. Sci. Lett. 141 (1996) 21–33.
[39] D.S. Wilson, R.N. Hey, C. Nishimura, Propagation as a mechanism of reorientation of the Juan de Fuca Ridge, J. Geophys. Res. 89 (1984) 9215–9225.
[40] W. Bach, E. Hegner, J. Erzinger, M. Satir, Chemical and isotopic variations along the superfast spreading East Pacific Rise from 6°–30°S, Contr. Min. Petr. 116 (1994) 365–380.
[41] H. Puchelt, R. Emmermann, Petrogenetic implications of tholeiitic basalt glasses from the East Pacific Rise and Galapagos spreading center, Chem. Geol. 38 (1983) 39–56.
[42] A.L. Rubin, D.D. Pollard, Dike-induced faulting in rift zones of Iceland and Afar, Geology 16 (1988) 413–416.